energies

MDPI

Article

Structural Evolution and Enhanced Piezoelectric Activity in Novel Lead-Free $BaTiO_3$-$Ca(Sn_{1/2}Zr_{1/2})O_3$ Solid Solutions

Ke Zhang [1], Pan Gao [1,*], Chang Liu [2,*], Xin Chen [1], Xinye Huang [1], Yongping Pu [2] and Zenghui Liu [3,*]

[1] School of Electronic Information and Artificial Intelligence, Shaanxi University of Science and Technology, Xi'an 710021, China
[2] School of Materials Science and Engineering, Shaanxi University of Science and Technology, Xi'an 710021, China
[3] Electronic Materials Research Laboratory, Key Laboratory of the Ministry of Education & International Center for Dielectric Research, School of Electronic Science and Engineering, Xi'an Jiaotong University, Xi'an 710049, China
* Correspondence: gaopan@sust.edu.cn (P.G.); liuchang@sust.edu.cn (C.L.); liu.z.h@xjtu.edu.cn (Z.L.)

Abstract: In this study, a series of solid solutions of $(1-x)BaTiO_3$-$xCa(Sn_{1/2}Zr_{1/2})O_3$ (abbreviated as $(1-x)$BT-xCSZ, x = 0.00–0.15) ceramics have been prepared by the conventional solid-state reaction method to search for high performance lead-free piezoelectric materials. The structural evolution, microstructure, and piezoelectric properties are investigated. X-ray diffraction (XRD) results indicate that the phase symmetry strongly depends on the CSZ content. A tetragonal phase is well-maintained in the compositions of $0 \leq x \leq 0.03$, and coexistence of tetragonal and cubic phases is obtained in the range of x = 0.06–0.09, beyond which a pure cubic phase becomes stable. More importantly, a significantly enhanced piezoelectric coefficient of $d_{33} = 388 \pm 9$ pC/N is attained in the composition of x = 0.06 in the MPB region, where a tetragonal ferroelectric phase and an ergodic relaxor phase with average cubic symmetry coexist. Based on the analysis of crystal structure and dielectric properties, a temperature-composition phase diagram consisting of four phase regions is established. This study indicates that the lead-free BT-CSZ binary system has great potential for use in electromechanical transducer applications.

Keywords: BT-based solid solutions; piezoelectric property; morphotropic phase boundary

Citation: Zhang, K.; Gao, P.; Liu, C.; Chen, X.; Huang, X.; Pu, Y.; Liu, Z. Structural Evolution and Enhanced Piezoelectric Activity in Novel Lead-Free $BaTiO_3$-$Ca(Sn_{1/2}Zr_{1/2})O_3$ Solid Solutions. *Energies* **2022**, *15*, 7795. https://doi.org/10.3390/en15207795

Academic Editor: Philippe Leclère

Received: 25 September 2022
Accepted: 19 October 2022
Published: 21 October 2022

1. Introduction

Piezoelectric material is capable of converting mechanical energy into electrical energy, and vice versa. For a long time, considerable attention has been paid to $Pb(Zr_{1-x}Ti_x)O_3$ (PZT) ceramics because of their admirable piezoelectric performance, which have been extensively utilized in actuating and sensing devices [1]. With the development of the electronics industry and growing environmental concerns, the use of toxic lead is restricted in many countries due to environmental and human health issues [2–4]. As a result, special attention has been paid to lead-free piezoelectric materials in order to replace the toxic PZT. Among the lead-free family, $BaTiO_3$ (BT) ceramic is the first man-made piezoelectric material, but it shows a relatively low piezoelectric coefficient (d_{33}) [5]. Subsequently, great efforts have been put into BT-based ceramics to optimize the piezoelectric properties; effective approaches are being explored, such as doping modification, microstructure design, domain engineering, mechanical imprint, and composite approach [6–14].

Among these methods, chemical doping on the perovskite A-site and B-site of BT ceramics to construct a multiphase boundary is particularly effective to obtain better piezoelectric properties. It is well-known that the enhanced piezoelectric responses in PZT are attributed to the morphotropic phase boundary (MPB), where different phases (such as rhombohedral, tetragonal, and monoclinic) coexist. The phase coexistence is believed to facilitate the polarization rotation among these phases, leading to an enhancement of

piezoelectric properties [15,16]. Similarly, an enhanced piezoelectric coefficient (d_{33}) has been observed in chemically modified BT-based ceramics by forming a phase boundary, which is comparable to that of PZT ceramics, triggering extensive studies on BT-based lead-free piezoelectric materials [17–23].

The construction of a phase boundary can be realized by optimizing the phase transition temperatures of BT-based ceramics, i.e., the rhombohedral-orthorhombic, orthorhombic-tetragonal, and tetragonal-cubic phase transition temperatures ($T_{R\text{-}O}$, $T_{O\text{-}T}$, and $T_{T\text{-}C}$). It has been shown that the phase transition temperatures can be tuned by replacing the A-site and/or B-site ions using isovalent elements, such as Ca, Zr, and Hf [24–29]. In particular, an enhanced piezoelectric property is expected when these phase transition temperatures become convergent at room temperature, where a phase boundary is formed near the triple point or quadruple compositions [30–37].

Although significant progress has been made in lead-free piezoelectric materials, their overall performances are still inferior to those of lead-based ones. Therefore, the objective of this study is to design novel lead-free piezoelectric materials with better piezoelectric properties. In this study, the replacement of Ca on the A-site and Zr/Sn on the B-site of the BT lattices has been performed to construct a phase boundary. A significantly enhanced piezoelectric property is found in the newly developed phase boundary, where the ferroelectric phase and the ergodic relaxor phase coexist.

2. Experimental Procedures

2.1. Materials Preparation

A series of the piezoceramics $(1-x)$BT-xCSZ with compositions x = 0–0.15 were fabricated by the conventional solid-state reaction route. Starting powders of barium carbonate ($BaCO_3$, 99%), calcium carbonate ($CaCO_3$, 99%), titanium dioxide (TiO_2, 99%), zirconium dioxide (ZrO_2, 99%), and stannic dioxide (SnO_2, 99%) were used as raw materials. All the reagent-grade powders were thoroughly mixed in proportion and ball-milled for 4 h with stabilized zirconia beads and ethanol as the mixing medium. The mixed powders were dried and then put into a furnace and calcined at 800 °C for 3 h in a sealed Al_2O_3 crucible. The calcined powders were ball-milled again for 4 h for better homogenization and mixed with a 5 wt% polyvinyl alcohol (PVA) solution. (The PVA solution worked as a binder and 7 drops of that were added to 5 g $(1-x)$BT-xCSZ powders approximatively). Then, the dried slurries were shaped into pellets of 6 mm in diameter and ~2.0 mm in thickness under uniaxial dry pressing at 10 MPa. The final sintering of the bulk piezoceramics was carried out at 1280–1420 °C depending on their composition for 3 h in air to form dense ceramics.

2.2. Characterization

The density of the sintered $(1-x)$BT-xCSZ ceramics was measured by the Archimedes water immersion method. The crystal structure and phase evolution were identified by X-ray diffraction (XRD, PANalytical Empyrean diffractometer, Almelo, The Netherlands) with a Cu-Kα1 X-ray radiation. The lattice parameters were calculated by the Rietveld refinements using the Topas Academic software. After sputtering gold on the polished and thermally etched surface, the microstructure of the sintered samples was examined by scanning electron microscopy, (SEM, FEI, Verios 460, Hillsboro, OR, USA). To characterize the electrical properties, the studied ceramics were further polished to ~0.5 mm in thickness and covered with silver paste on both surfaces as electrodes. The permittivity and loss factor were measured under different frequencies using a computer-controlled programmable furnace with an LCR meter (Agilent, E4980A, Santa Clara, CA, USA) in the temperature range of 30 °C to 300 °C. The polarization-electric field (P-E) hysteresis loops were recorded at room temperature by a ferroelectric test system (TF Analyzer 2000, aixACCT, Aachen, Germany) at a frequency of 10 Hz. After poling under a DC electric field of 3 kV/mm at room temperature for 10 min, the piezoelectric coefficient d_{33} was measured using a quasi-static d_{33} testing meter (ZJ-3AN, CAS, Beijing, China).

3. Results and Discussion

3.1. Bulk Density

The relationship between the relative density of the $(1-x)$BT-xCSZ ceramics and the sintering temperature was investigated. The relative density of the $(1-x)$BT-xCSZ ceramics increased initially and then dropped with increasing sintering temperature, as displayed in Figure 1, suggesting the existence of an optimum sintering temperature (OST) for each composition.

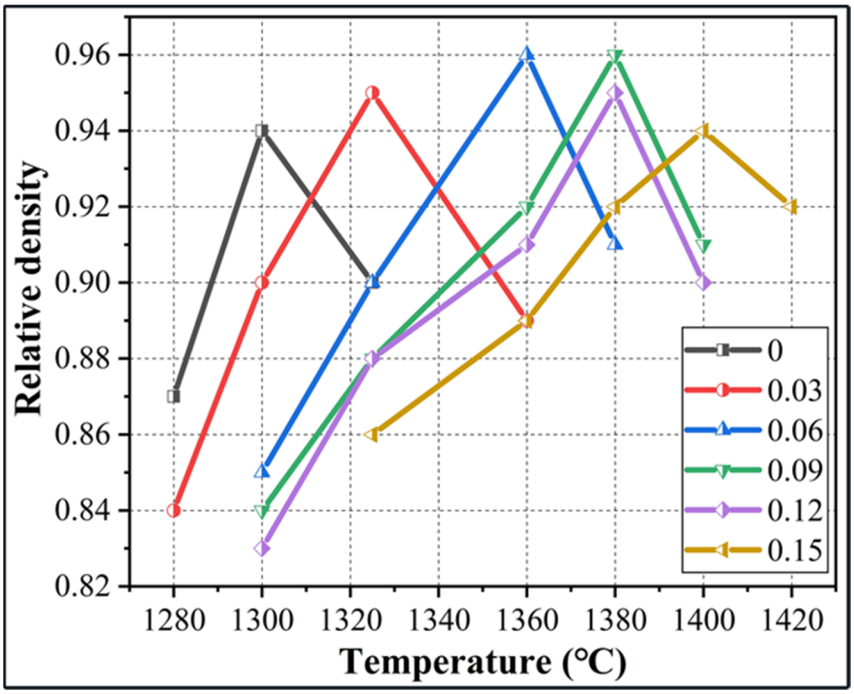

Figure 1. The relative density of the $(1-x)$BT-xCSZ ceramics as a function of sintering temperature.

The $(1-x)$BT-xCSZ ceramics exhibit a number of pores below the OST, above which an over-sintering phenomenon appears. Both of these cases worsen the densification of the ceramics. The relative density of all the samples at the OST is greater than 94%, indicating good sinterability in the samples.

As shown in Figure 1, the OSTs of the $(1-x)$BT-xCSZ ceramics for x = 0, 0.03, 0.06, 0.09, 0.12, and 0.15 are 1300 °C, 1325 °C, 1360 °C, 1380 °C, 1380 °C, and 1400 °C, respectively. Therefore, a higher sintering temperature is required after doping CSZ in the BT-based ceramics.

3.2. Microstructure

Figure 2 shows the SEM surface micrographs of the $(1-x)$BT-xCSZ ceramics with x = 0, 0.03, 0.06, 0.09, 0.12, and 0.15 sintered at their respective OST. It can be seen that all the ceramics show a compacted microstructure without any obvious pores. The average grain size of the CSZ-doped BT ceramics was checked by using Nano Measurer software. After calculation by the linear intercept method on SEM images, the average grain size of the samples was determined to be about 26.5 ± 1.5 μm for undoped BT ceramics, and it drops dramatically to 13.2 ± 0.5 μm for 0.85BT-0.15CSZ ceramics with the increasing CSZ content. Therefore, the average grain size is highly relevant with the CSZ concentration. The decreased grain size is due to the introduction of Ca^{2+}, Zr^{4+}, and Sn^{4+} with larger ionic radii, which have low ionic mobility during sintering, and as a result, inhibit the grain growth [38].

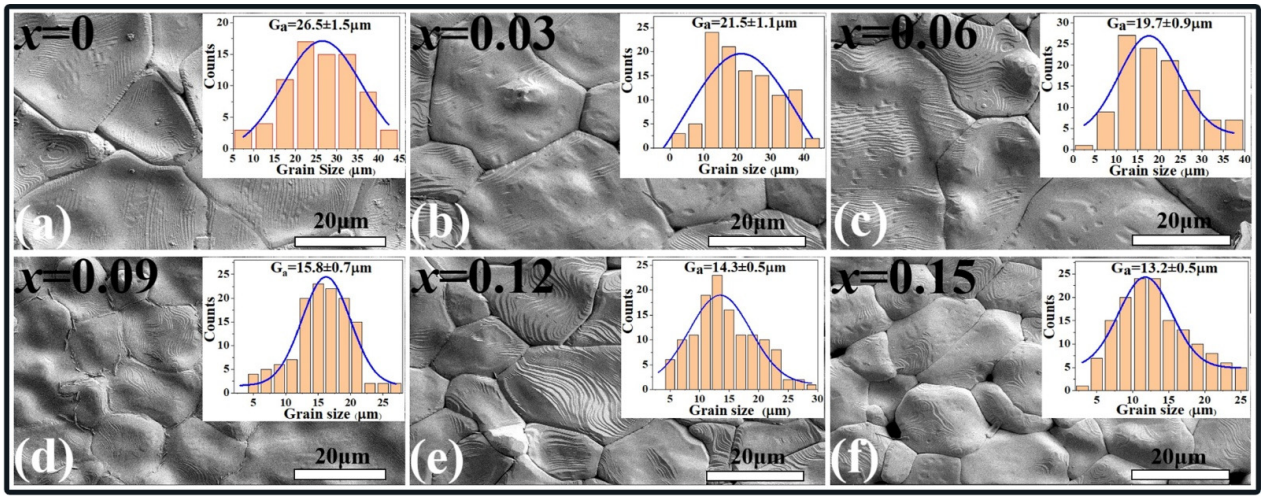

Figure 2. SEM morphologies of the (1−*x*)BT-*x*CSZ ceramics with (**a**) *x* = 0, (**b**) *x* = 0.03, (**c**) *x* = 0.06, (**d**) *x* = 0.09, (**e**) *x* = 0.12, and (**f**) *x* = 0.15.

3.3. Crystal Structure

To study the crystal structures and composition-induced phase transition behavior of the (1−*x*)BT-*x*CSZ ceramics, the XRD patterns of the sintered samples with different compositions (*x* = 0.00–0.15) were measured at room temperature, as presented in Figure 3. The characteristic diffraction peaks in Figure 3a reveal the formation of a pure perovskite structure for all the compositions, indicating that the CSZ dopant has diffused completely into the BT lattice to form homogeneous solid solutions without any impurity phases.

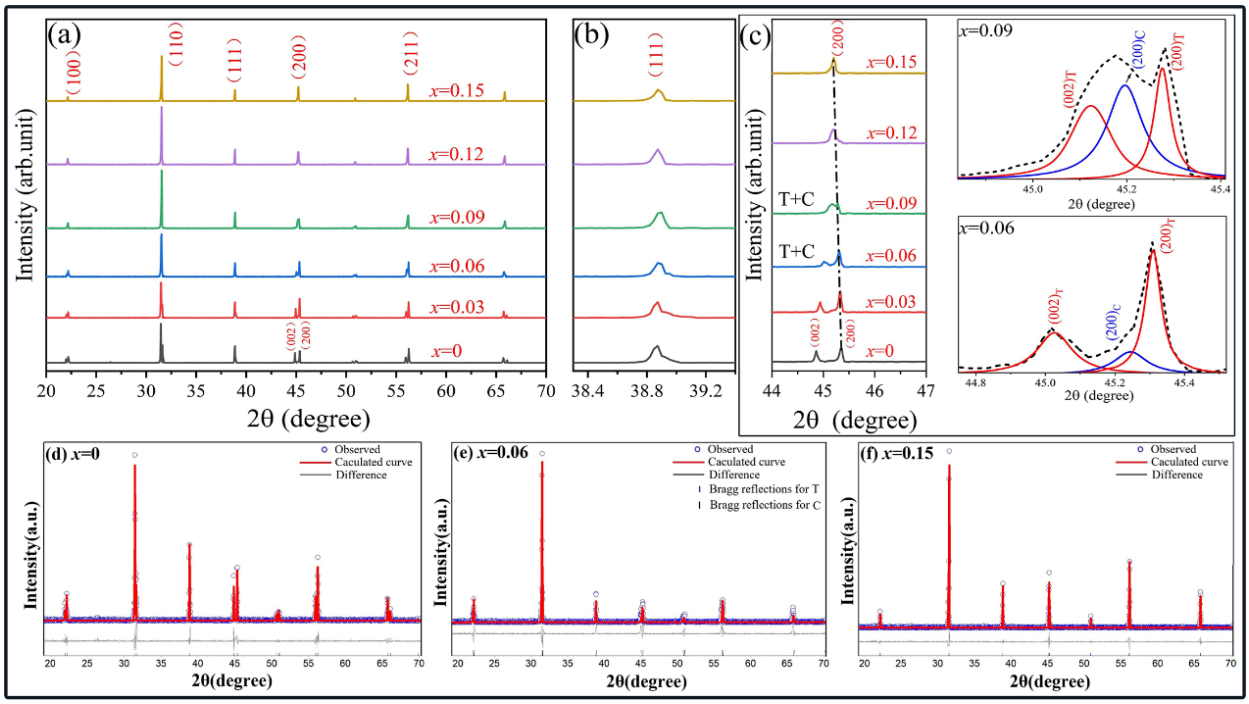

Figure 3. XRD patterns of (**a**) the as-sintered (1−*x*)BT-*x*CSZ ceramics with different compositions, (**b**) the amplified patterns at 2*θ* = 38.4~39.2°, (**c**) the enlarged XRD patterns of the (200)/(002) peaks and the peak fitting in *x* = 0.06 and 0.09, (**d**–**f**) Rietveld refinement results of the (1−*x*)BT-*x*CSZ ceramics with *x* = 0, *x* = 0.06 and *x* = 0.15 at room temperature.

Obviously, the ceramics with x = 0–0.03 exhibit a typical tetragonal structure as characterized by the splitting (200)/(002) peaks and a single (111) peak. With the increasing CSZ content, the (111) peak remains almost unchanged (Figure 3b). In comparison, the (200) diffraction peaks gradually broaden in the compositions of x = 0.06–0.09. The (200) and (002) peaks merge into a single peak when the CSZ content increases further to x = 0.12–0.15, indicating the stabilization of a cubic phase in these compositions.

The enlarged XRD patterns of the (200)/(002) peaks of x = 0.06 and 0.09 are given in Figure 3c. Both of their (200)/(002) peaks can be well fitted with three peaks, indicating that these compositions are located in the MPB region. The MPB region can be regarded as a structural bridge between the tetragonal and cubic phases, where these two phases have equal free energy and coexist uniformly.

In order to clarify the detailed structural evolution of the prepared $(1-x)$BT-xCSZ ceramics, Rietveld refinements for the ceramics with x = 0, 0.15, and 0.06 were carried out using the tetragonal *P4mm*, cubic $Pm\bar{3}m$, and *P4mm* + $Pm\bar{3}m$ model, respectively. The refined results are shown in Figure 3d–f. It can be seen that the calculated curves agree well with the observed XRD diffraction profiles, indicating the high reliability of the refined results.

With these observations, we conclude that the crystal structure of the $(1-x)$BT-xCSZ solid solutions changes from a tetragonal *P4mm* phase to an MPB region with *P4mm* and $Pm\bar{3}m$ phases, and finally turns out to be a cubic $Pm\bar{3}m$ phase.

Compared with pure BT, it is noted that the (200) peak of the $(1-x)$BT-xCSZ solid solutions gradually shifts to a lower 2θ degree, indicating the expansion of the unit cells. The expansion of the unit cells arises from the larger ionic radii of Ca^{2+}, Zr^{4+}, and Sn^{4+} than those of Ba^{2+} and Ti^{4+}.

The crystal structure and the calculated lattice parameters as a function of x from the refinement results are listed in Table 1. One can notice that the lattice parameters a and b increase, whereas c decreases with increasing CSZ concentration. Therefore, the tetragonality (c/a ratio) of the *P4mm* phase decreases from 1.01 for pure BT ceramics to 1.003 for the x = 0.06 ceramics and then to 1.00 for the ceramics with higher x values, suggesting the degradation of the *P4mm* phase.

Table 1. The crystal structure and refined lattice parameters of $(1-x)$BT-xCSZ ceramics.

Component		**0**	**0.06**		**0.15**
Symmetry		T	T + C		C
Space group		*P4mm*	*P4mm*	$Pm\bar{3}m$	$Pm\bar{3}m$
Lattice parameters parameters	a (Å)	3.995 (3)	4.008 (8)	4.011 (2)	4.014 (1)
	b (Å)	3.995 (3)	4.008 (8)	4.011 (2)	4.014 (1)
	c (Å)	4.035 (2)	4.021 (1)	4.011 (2)	4.014 (1)
	c/a	1.010	1.003 (2)	1.000	1.000
Cell volume	V (Å^3)	64.399 (7)	64.594 (6)	64.529 (4)	64.674 (3)

The effects of the CSZ content on the structural evolution, phase boundary, and lattice parameters calculated from the Rietveld refinements of the BT-based ceramics are shown in Figure 4. As the CSZ concentration increases, a gradual phase transition sequence from tetragonal to MPB, and then to cubic, is clearly revealed.

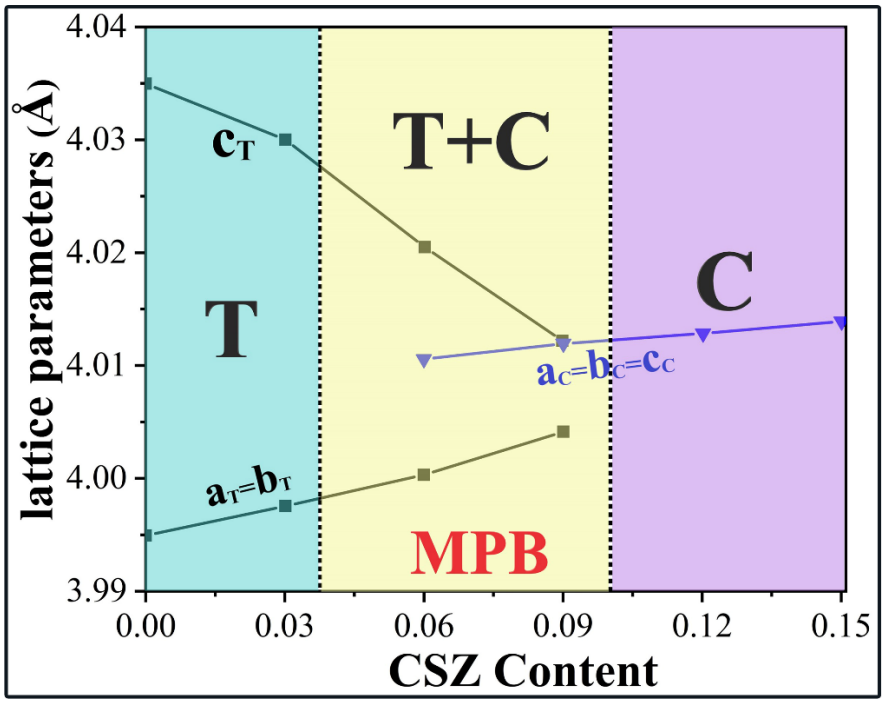

Figure 4. Variations of the crystal structure and lattice parameters as a function of CSZ content for the (1−*x*)BT-*x*CSZ ceramics at room temperature.

3.4. Dielectric and Phase Transition Behavior

The permittivity and loss factor of the (1−*x*)BT-*x*CSZ (*x* = 0, 0.03, 0.06, 0.09, 0.12, and 0.15) ceramics at frequencies of 1 kHz to 1 MHz are plotted as a function of temperature, as illustrated in Figure 5. In pure BT ceramic, a sharp dielectric peak independent of frequency is found at $T_c = T_m$ = 125 °C, corresponding to the phase transition temperature from the ferroelectric tetragonal (*P4mm*) to the paraelectric cubic ($Pm\bar{3}m$) phases (Curie temperature T_c) in normal ferroelectric materials. Here T_m refers to the temperature where the permittivity reaches its maximum. The T_c/T_m decreases to 110 °C in *x* = 0.03.

With the increasing CSZ content (*x* = 0.06 and *x* = 0.09), a shoulder gradually develops at the temperature below T_m, and it shifts to a lower temperature as shown in the insert of Figure 5c,d. At the same time, the samples start to show some relaxor behaviors as evidenced by the observation that T_m gradually shifts to higher temperatures with increasing frequency. As a result, a temperature-induced spontaneous transformation from the ferroelectric to ergodic relaxor phases occurs at T_c in *x* = 0.06 and *x* = 0.09. A similar phenomenon was also found in PZ-PT-BZN and PMN-BZN-PT systems [39–41].

With further increase in the CSZ content, the dielectric curves become evenly diffused, and the value of T_m shows a strong dependence on frequency (Figure 5g–i), suggesting an enhanced relaxor behavior [42,43]. In the compositions of *x* = 0.12 and 0.15, the dielectric anomaly at T_c disappears, and an ergodic relaxor phase shows up at room temperature.

In relaxor ferroelectrics, the Curie–Weiss law ($\varepsilon = C/(T - T_{CW})$, where ε, C, T, and T_{CW} stands for permittivity, Curie–Weiss constant, measured temperature, and Curie–Weiss temperature, respectively) is found to be satisfied at $T > T_b$ (Burns temperature), where the crystal is of paraelectric (PE) nature. Therefore, by fitting the dielectric curve with the Curie–Weiss law, T_b can be obtained, which determines the phase boundary between the ergodic relaxor state and the paraelectric state.

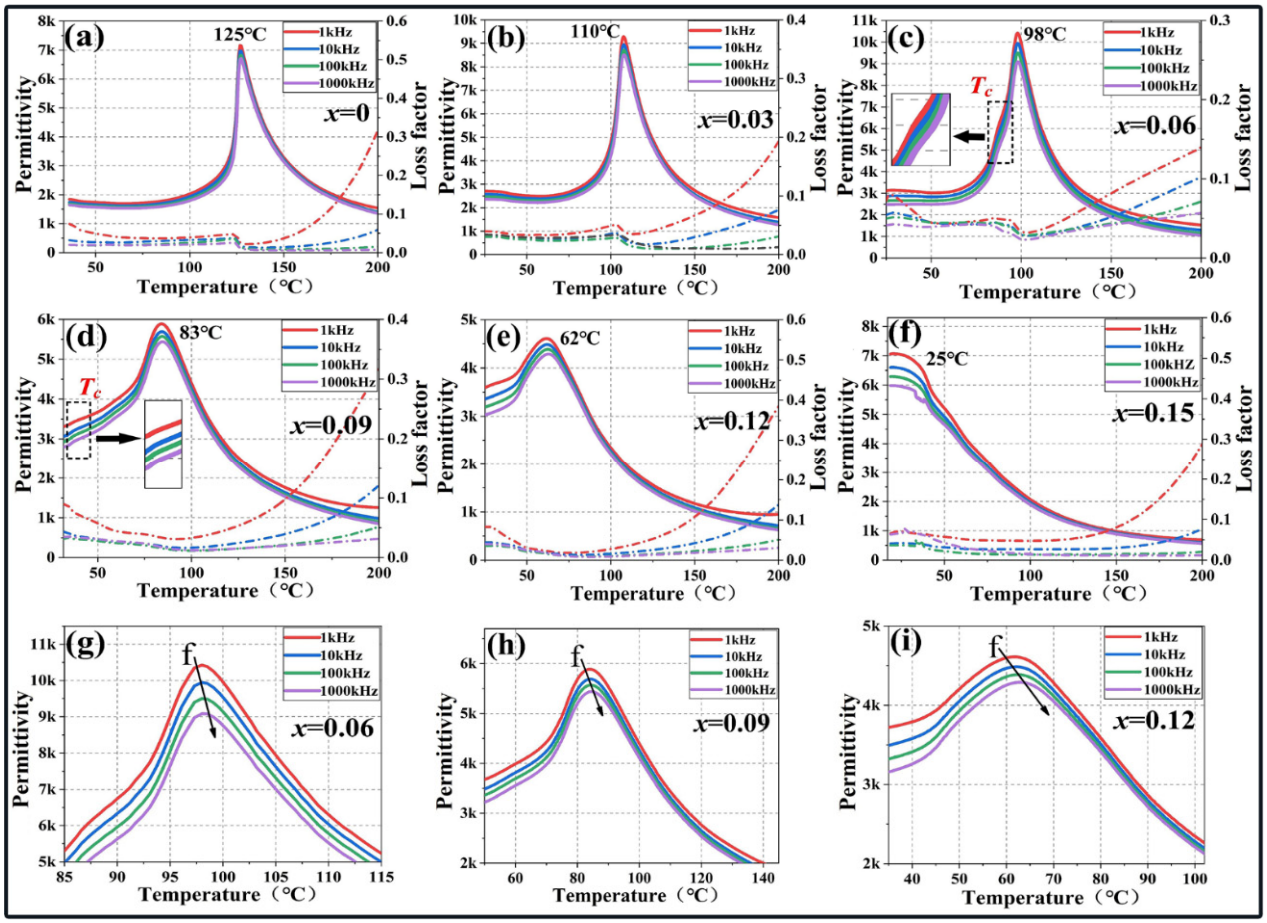

Figure 5. (**a**–**f**) Permittivity and loss factor of the $(1-x)$BT-xCSZ ($0 \leq x \leq 0.15$) ceramics measured at various frequencies. (**g**–**i**) Enlarged view of the dielectric peaks for the $(1-x)$BT-xCSZ ceramics with x = 0.06, 0.09 and 0.12.

3.5. Ferroelectric Properties

To further investigate the polarization and phase transition behavior driven by the CSZ dopant, the hysteresis loops of the $(1-x)$BT-xCSZ ceramics were measured at 10 Hz under various applied fields, as shown in Figure 6a–g. The pure BT ceramic exhibits a saturated *P-E* hysteresis loop under ±50 kV/cm. With the increase in a small amount of CSZ content, the *P-E* hysteresis loop becomes well squared (e.g., x = 0.03 and 0.06), indicating a good ferroelectricity at room temperature. With a further increase in the CSZ content, the shapes of the *P-E* hysteresis loops gradually change from well-squared loops to slim loops, which are characteristic of relaxors.

The values of P_{max}, P_r, and E_c versus composition x for the studied ceramics are displayed in Figure 6h,i. Both the maximum polarization (P_{max}) and remanent polarization (P_r) measured under 40 kV/cm show an increasing trend first and then decrease with the increasing CSZ content. The increase in P_{max} and P_r can be attributed to the phase transformation from a single tetragonal phase to the coexistence of cubic and tetragonal phases, which leads to an easier reorientation of the polarization vectors between different accepted directions and the possible polarization extension due to the flattening of the free energy profile in the MPB region [17,18].

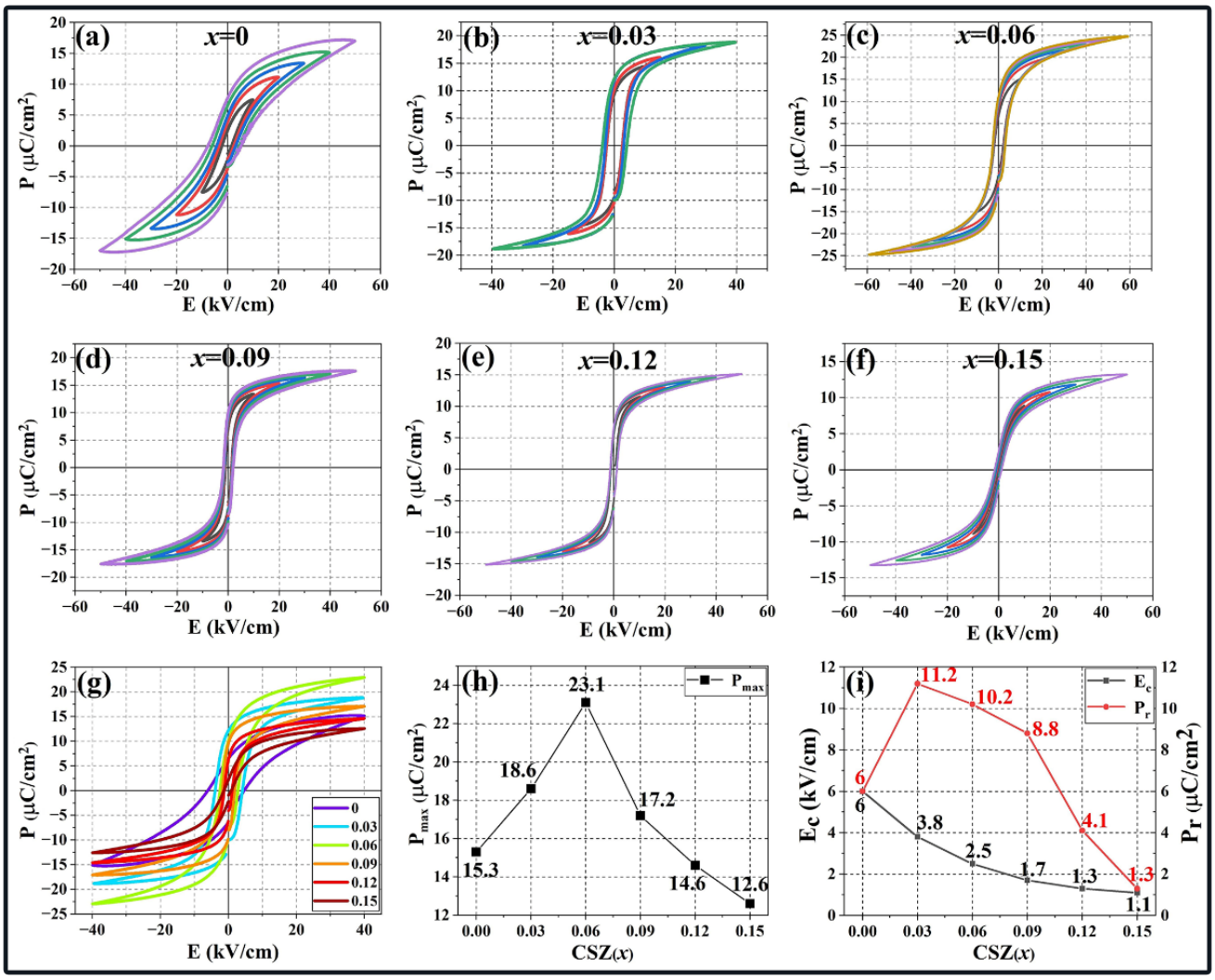

Figure 6. Polarization-electric field hysteresis loops measured at room temperature under different electric-field for the $(1-x)$BT-xCSZ ceramics: (**a**) x = 0, (**b**) x = 0.03, (**c**) x = 0.06, (**d**) x = 0.09, (**e**) x = 0.12, and (**f**) x = 0.15. (**g**) The P-E loops of the studied ceramics measured at ±40 kV/cm. (**h**,**i**) Evolution of the P_{max}, P_r, and E_c value as a function of the CSZ content.

Further increasing the CSZ content leads to the degeneration of the P_r values from 10.2 μC/cm^2 (x = 0.06) to 1.3 μC/cm^2 (x = 0.15) for the $(1-x)$BT-xCSZ ceramics, as shown in Figure 6i. The gradual slimming P-E hysteresis loops with smaller P_r are coupled to the enhanced relaxor behavior, as shown in Figure 5g–i.

Moreover, the values of coercive field E_c show a decreasing trend with the increase in CSZ content, which might be related to the increasing presence of the cubic phase and the nanosized domains in the ergodic relaxor state. The nanodomains in the ergodic relaxor state are more responsive to the external electric field than are the macroscopic domains in the ferroelectric state, usually resulting in a slimmer hysteresis loop [44].

3.6. Phase Diagram and Piezoelectric Properties

Based on the analysis of the crystal structure and the dielectric property, a temperature-composition phase diagram of the $(1-x)$BT-xCSZ ceramics is proposed, as illustrated in Figure 7. The phase diagram studied in this work shows different phase structures and phase transition sequences, consisting of four phase regions, T, T + C (MPB), ER (ergodic relaxor) and cubic phases. With the increasing CSZ content, the tetragonal phase is suppressed with the decreasing tetragonality c/a. It seems that the change of c/a is mainly

influenced by the substitution of Sn^{4+} and Zr^{4+} for Ti^{4+} ions, because the replacement of Ca^{2+} for Ba^{2+} ion on the A-site has negligible effects on the T_c value [44]. It is noted that the range of the ergodic relaxor phase between T_c and T_b gradually widens, further confirming the enhanced relaxor behavior. The MPB region with the coexistence of C and T phases appears in the composition of $0.06 \leq x \leq 0.09$.

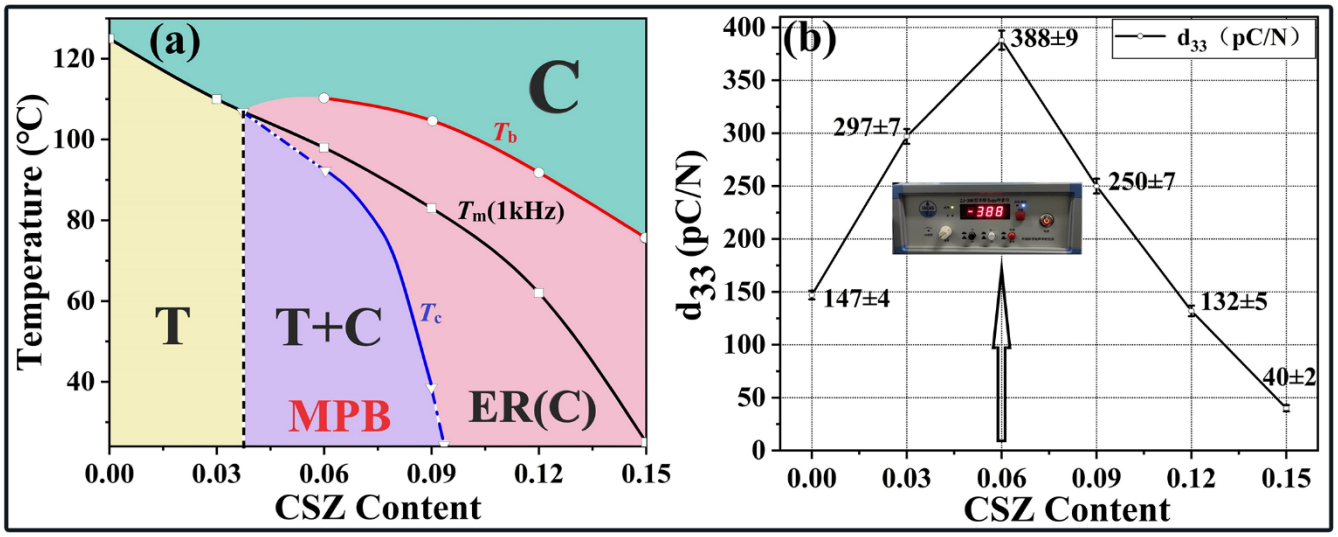

Figure 7. (**a**) phase diagram and (**b**) d_{33} values of the $(1-x)$BT-xCSZ ceramics as a function of x.

Figure 7b presents the piezoelectric coefficient of the BT-based ceramics as a function of CSZ content. The value of d_{33} increases and reaches a maximum value of 388 ± 9 pC/N in the composition of $x = 0.06$ (in the MPB region), and then decreases with the increasing x. The significantly enhanced piezoelectric coefficient indicates that constructing a phase boundary is an effective way to design lead-free materials with good piezoelectricity.

It should be pointed that noticeable piezoelectricity is observed in the compositions of $x > 0.09$, which have been determined to be cubic in symmetry by XRD. Therefore, the phase in these compositions is not a real cubic structure at room temperature. Instead, it is a phase with a local polar structure in micro-/nanoscale but with cubic symmetry on average. By applying an electric field (poling), long-range polar order is induced, leading to a detectable macroscopic piezoelectric response [45]. Such a short-range polar structure has been revealed in some relaxor ferroelectrics [46,47]. Further investigations are underway to clarify the relationship between the multiscale structure and electromechanical properties in the $(1-x)$BT-xCSZ ceramics.

4. Conclusions

In this study, ceramics of the $(1-x)$BT-xCSZ binary solid solutions have been synthesized by the conventional solid-state reaction method. The effects of CSZ substitution on the crystal structure, dielectric, and piezoelectric properties of the BT ceramics are investigated. With increasing CSZ content, the structure changes from a tetragonal phase to the MPB regions with a mixture of tetragonal and cubic phases, and then toward a cubic phase. The as-prepared $(1-x)$BT-xCSZ ceramics exhibit dense microstructure. An enhanced relaxor behavior is indicated with the substitution of CSZ. More importantly, a significantly enhanced piezoelectric coefficient of $d_{33} = 388 \pm 9$ pC/N is attained in the composition of $x = 0.06$ in the MPB region, where a tetragonal ferroelectric phase and an ergodic relaxor phase with average cubic symmetry coexist. On the basis of the crystal structure and dielectric property analysis, a temperature-composition phase diagram consisting of four phase regions (i.e., tetragonal ferroelectric, MPB ferroelectric, cubic ergodic relaxor, and cubic paraelectric) is established. Our results demonstrate that the newly developed BT-CSZ solid solutions are an attractive lead-free material family for electromechanical transducer applications.

Author Contributions: Preparation and performing of the experiments, electrical properties measurements, manuscript's writing—origin draft, K.Z.; paper idea, experimental designing, data analysis, manuscript writing—review & editing, P.G., C.L. and Z.L.; experimental investigation and data processing, X.C. and X.H.; data analysis, language polishing, Z.L. and Y.P. All authors have read and agreed to the published version of the manuscript.

Funding: This study was supported by the National Natural Science Foundation of China (Grant Nos. 52202142 and 51902244), the Natural Science Basic Research Program of Shaanxi Province (Grants Nos. 2022JQ-337 and 2020JQ-710), the Doctoral Scientific Research Startup Foundation of Shaanxi University of Science and Technology (Grants Nos. 2019QNBJ-12 and 2018BJ-07), and the Fundamental Research Funds for the Central Universities of China (Grant No. xzy012021025).

Data Availability Statement: Not applicable.

Acknowledgments: The authors thank Zhixuan Guo for the XRD measurements.

Conflicts of Interest: The authors declare no conflict of interest.

References

1. Jaffe, H. Piezoelectric ceramics. *J. Am. Ceram. Soc.* **1958**, *41*, 494–498. [CrossRef]
2. Li, J.F.; Wang, K.; Zhu, F.Y.; Cheng, L.Q.; Yao, F.Z. (K,Na)NbO_3-Based Lead-Free Piezoceramics: Fundamental Aspects, Processing Technologies, and Remaining Challenges. *J. Am. Ceram. Soc.* **2013**, *96*, 3677–3696. [CrossRef]
3. McFarland, M.J.; Hauer, M.E.; Reuben, A. Half of US population exposed to adverse lead levels in early childhood. *Proc. Natl. Acad. Sci. USA* **2022**, *119*, e2118631119. [CrossRef]
4. Directive, E.U. Restriction of the use of certain hazardous substances in electrical and electronic equipment (RoHS). *Off. J. Eur. Communities* **2013**, *46*, 19–23.
5. Bechmann, R. Elastic, piezoelectric and dielectric constants of polarized barium titanate ceramics and some applications of the piezoelectric equations. *J. Acoust. Soc. Am.* **1956**, *28*, 347–350. [CrossRef]
6. Liu, H.; Liu, Y.-X.; Song, A.; Li, Q.; Yin, Y.; Yao, F.Z.; Wang, K.; Gong, W.; Zhang, B.P.; Li, J.F. (K,Na)NbO_3-based lead-free piezoceramics: One more step to boost applications. *Natl. Sci. Rev.* **2022**, *9*, nwac101. [CrossRef]
7. Zhang, S.W.; Zhang, H.; Zhang, B.P.; Yang, S. Phase-transition behavior and piezoelectric properties of lead-free $(Ba_{0.95}Ca_{0.05})(Ti_{1-x}Zr_x)O_3$ ceramics. *J. Alloys Compd.* **2010**, *506*, 131–135. [CrossRef]
8. Roy, P.K.; Ponraj, B.; Varma, K.B.R. Dielectric, ferroelectric and piezoelectric properties of $(Ba_{0.98-x}Sr_xCa_{0.02})(Ti_{0.95}Zr_{0.05})O_3$ lead-free ceramics. *Ceram. Int.* **2017**, *43*, 15762–15768. [CrossRef]
9. Liang, D.; Zhu, X.; Zhang, Y.; Shi, W.; Zhu, J. Large piezoelectric effect in (1-*x*)$Ba(Zr_{0.15}Ti_{0.85})O_3$-*x*$(Ba_{0.8}Sr_{0.2})TiO_3$ lead-free ceramics. *Ceram. Int.* **2015**, *41*, 8261–8266. [CrossRef]
10. Wang, D.; Jiang, Z.; Yang, B.; Zhang, S.; Zhang, M.; Guo, F.; Cao, W. Phase transition behavior and high piezoelectric properties in lead-free $BaTiO_3$-$CaTiO_3$-$BaHfO_3$ ceramics. *J. Mater. Sci.* **2014**, *49*, 62–69. [CrossRef]
11. Zhu, L.F.; Zhang, B.P.; Zhao, L.; Li, S.; Zhou, Y.; Shi, X.C.; Wang, N. Large piezoelectric effect of (Ba,Ca)TiO_3-*x*$Ba(Sn,Ti)O_3$ lead-free ceramics. *J. Eur. Ceram. Soc.* **2016**, *36*, 1017–1024. [CrossRef]
12. Marton, P.; Rychetsky, I.; Hlinka, J. Domain walls of ferroelectric $BaTiO_3$ within the Ginzburg-Landau-Devonshire phenomenological model. *Phys. Rev. B.* **2010**, *81*, 144125. [CrossRef]
13. Höfling, M.; Zhou, X.; Riemer, L.M.; Bruder, E.; Liu, B.; Zhou, L.; Rödel, J. Control of polarization in bulk ferroelectrics by mechanical dislocation imprint. *Science* **2021**, *372*, 961–964. [CrossRef] [PubMed]
14. Wu, H.; Zhuo, F.; Qiao, H.; Kodumudi Venkataraman, L.; Zheng, M.; Wang, S.; Zhang, Q. Polymer-/Ceramic-based Dielectric Composites for Energy Storage and Conversion. *EEM* **2022**, *5*, 486–514. [CrossRef]
15. Fu, H.; Cohen, R.E. Polarization rotation mechanism for ultrahigh electrome-chanical response in single-crystal piezoelectrics. *Nature* **2000**, *403*, 281–283. [CrossRef] [PubMed]
16. Wu, J.; Xiao, D.; Zhu, J. Potassium-sodium niobate lead-free piezoelectric materials: Past, present, and future of phase boundaries. *Chem. Rev.* **2015**, *115*, 2559–2595. [CrossRef]
17. Xue, D.; Zhou, Y.; Bao, H.; Gao, J.; Zhou, C.; Ren, X. Large piezoelectric effect in Pb-free $Ba(Ti,Sn)O_3$-*x*$(Ba,Ca)TiO_3$ ceramics. *Appl. Phys. Lett.* **2011**, *99*, 122901. [CrossRef]
18. Damjanovic, D. A morphotropic phase boundary system based on polarization rotation and polarization extension. *Appl. Phys. Lett.* **2010**, *97*, 062906. [CrossRef]
19. Zhou, C.; Liu, W.; Xue, D.; Ren, X.; Bao, H.; Gao, J.; Zhang, L. Triple-point-type morphotropic phase boundary based large piezoelectric Pb-free material-$Ba(Ti_{0.8}Hf_{0.2})O_3$-$(Ba_{0.7}Ca_{0.3})TiO_3$. *Appl. Phys. Lett.* **2012**, *22*, 222910. [CrossRef]
20. Tian, Y.; Wei, L.; Chao, X.; Liu, Z.; Yang, Z. Phase transition behavior and large piezoelectricity near the morphotropic phase boundary of lead-free $(Ba_{0.85}Ca_{0.15})(Zr_{0.1}Ti_{0.9})O_3$ ceramics. *J. Am. Ceram. Soc.* **2013**, *96*, 496–502. [CrossRef]
21. Wang, D.; Jiang, Z.; Yang, B.; Zhang, S.; Zhang, M.; Guo, F.; Cao, W. Phase diagram and enhanced piezoelectric response of lead-free $BaTiO_3$-$CaTiO_3$-$BaHfO_3$ system. *J. Am. Ceram. Soc.* **2014**, *97*, 3244–3251. [CrossRef]

22. Janbua, W.; Bongkarn, T.; Kolodiazhnyi, T.; Vittayakorn, N. High piezoelectric response and polymorphic region in the lead-free piezoelectric $BaTiO_3$-$CaTiO_3$-$BaSnO_3$ ternary system. *RSC Adv.* **2017**, *7*, 30166–30176. [CrossRef]
23. Cordero, F.; Craciun, F.; Dinescu, M.; Scarisoreanu, N.; Galassi, C.; Schranz, W.; Soprunyuk, V. Elastic response of (1-*x*)$Ba(Ti_{0.8}Zr_{0.2})O_3$-*x*$(Ba_{0.7}Ca_{0.3})TiO_3$ (*x* = 0.45-0.55) and the role of the intermediate orthorhombic phase in enhancing the piezoelectric coupling. *Appl. Phys. Lett.* **2014**, *105*, 232904. [CrossRef]
24. Elbasset, A.; Sayouri, S.; Abdi, F.; Lamcharfi, T.; Mrharrab, L. Effect of Sr addition on piezoelectric properties and the transition temperature of $BaTiO_3$. *Glass Phys. Chem.* **2017**, *43*, 91–97. [CrossRef]
25. Zhang, L.; Zhang, M.; Wang, L.; Zhou, C.; Zhang, Z.; Yao, Y.; Zhang, L.; Xue, D.; Lou, X.; Ren, X. Phase transitions and the piezoelectricity around morphotropic phase boundary in $Ba(Zr_{0.2}Ti_{0.8})O_3$-*x*$(Ba_{0.7}Ca_{0.3})TiO_3$ lead-free solid solution. *Appl. Phys. Lett.* **2014**, *105*, 162908. [CrossRef]
26. Acosta, M.; Novak, N.; Jo, W.; Rödel, J. Relationship between electromechanical properties and phase diagram in the $Ba(Zr_{0.2}Ti_{0.8})O_3$-*x*$(Ba_{0.7}Ca_{0.3})TiO_3$ lead-free piezoceramic. *Acta Mater.* **2014**, *80*, 48–55. [CrossRef]
27. Nahas, Y.; Akbarzadeh, A.; Prokhorenko, S.; Prosandeev, S.; Walter, R.; Kornev, I.; Iniguez, J.; Bellaiche, L. Microscopic origins of the large piezoelectricity of lead free (Ba,Ca)(Zr,Ti)O_3. *Nat. Commun.* **2017**, *8*, 15944. [CrossRef]
28. Abebe, M.; Brajesh, K.; Mishra, A.; Senyshyn, A.; Ranjan, R. Structural perspective on the anomalous weak-field piezoelectric response at the polymorphic phase boundaries of (Ba,Ca)(Ti,M)O_3 lead-free piezoelectrics (*M* = Zr, Sn, Hf). *Phys. Rev. B.* **2017**, *96*, 014113. [CrossRef]
29. Li, H.R.; Chen, C.X.; Zheng, R.K. Effects of Sr substitution on the structural, dielectric, ferroelectric, and piezoelectric properties of Ba(Zr,Ti)O_3 lead-free ceramics. *J. Mater. Sci. Mater. Electron.* **2015**, *26*, 3057–3063. [CrossRef]
30. Liu, W.; Ren, X. Large piezoelectric effect in Pb-free ceramics. *Phys. Rev. Lett.* **2009**, *103*, 257602. [CrossRef] [PubMed]
31. Zhao, C.; Wu, H.; Li, F.; Cai, Y.; Zhang, Y.; Song, D.; Wu, J.; Lu, X.; Yin, J.; Xiao, D.; et al. Practical high piezoelectricity in barium titanate ceramics utilizing multiphase convergence with broad structural flexibility. *J. Am. Chem. Soc.* **2018**, *140*, 15252–15260. [CrossRef] [PubMed]
32. Gao, J.; Xue, D.; Wang, Y.; Wang, D.; Zhang, L.; Wu, H.; Guo, S.; Bao, H.; Zhou, C.; Liu, W.; et al. Microstructure basis for strong piezoelectricity in Pb-free Ba $(Zr_{0.2}Ti_{0.8})O_3$-$(Ba_{0.7}Ca_{0.3})TiO_3$ ceramics. *Appl. Phys. Lett.* **2011**, *99*, 092901. [CrossRef]
33. Gao, J.; Dai, Y.; Hu, X.; Ke, X.; Zhong, L.; Li, S.; Zhang, L.; Wang, Y.; Wang, D.; Wang, Y.; et al. Phase transition behaviours near the triple point for Pb-free (1-*x*)$Ba(Zr_{0.2}Ti_{0.8})O_3$-*x*$(Ba_{0.7}Ca_{0.3})TiO_3$ piezoceramics. *Europhys. Lett.* **2016**, *115*, 37001. [CrossRef]
34. Zhu, L.F.; Zhang, B.P.; Zhao, X.K.; Zhao, L.; Yao, F.Z.; Han, X.; Zhou, P.F.; Li, J.F. Phase transition and high piezoelectricity in $(Ba,Ca)(Ti_{1-x}Sn_x)O_3$ lead-free ceramics. *Appl. Phys. Lett.* **2013**, *103*, 072905. [CrossRef]
35. Wang, D.; Fan, Z.; Rao, G.; Wang, G.; Liu, Y.; Yuan, C.; Ma, T.; Li, D.; Tan, X.; Lu, Z.; et al. Ultrahigh piezoelectricity in lead-free piezoceramics by synergistic design. *J. Nano Energy Power Res.* **2020**, *76*, 104944. [CrossRef]
36. Yan, S.; Cao, Z.; Liu, Q.; Gao, Y.; Zhang, H.; Li, G. Enhanced piezoelectric activity around orthorhombic-tetragonal phase boundary in multielement codoping $BaTiO_3$. *J. Alloys Compd.* **2022**, *923*, 166398. [CrossRef]
37. Keeble, D.S.; Benabdallah, F.; Thomas, P.A.; Maglione, M.; Kreisel, J. Revised structural phase diagram of $(Ba_{0.7}Ca_{0.3}TiO_3)$-$(BaZr_{0.2}Ti_{0.8}O_3)$. *Appl. Phys. Lett.* **2013**, *102*, 092903. [CrossRef]
38. Wang, H.; Yuan, H.; Li, X.; Zeng, F.; Wu, K.; Zheng, Q.; Fan, G.; Lin, D. Enhanced energy density and discharged efficiency of Lead-Free relaxor (1-*x*)$[(Bi_{0.5}Na_{0.5})_{0.94}Ba_{0.06}]_{0.98}La_{0.02}TiO_3$-*x*$KNb_{0.6}Ta_{0.4}O_3$ Ceramic Capacitors. *Chem. Eng. J.* **2020**, *394*, 124879. [CrossRef]
39. Liu, Z.; Gao, P.; Wu, H.; Ren, W.; Ye, Z.-G. Synthesis, structure, and properties of the $PbZrO_3$-$PbTiO_3$-$Bi(Zn_{2/3}Nb_{1/3})O_3$ ternary solid solution system around the morphotropic phase boundary. *Phys. Status Solidi A* **2018**, *215*, 1701007. [CrossRef]
40. Liu, Z.; Wu, H.; Ren, W.; Ye, Z.-G. Complex morphotropic phase transformations and high piezoelectric properties in new ternary perovskite single crystals. *Acta Mater.* **2018**, *149*, 132–141. [CrossRef]
41. Liu, Z.; Paterson, A.R.; Wu, H.; Gao, P.; Ren, W.; Ye, Z.-G. Synthesis, structure and piezo-/ferroelectric properties of a novel bismuth-containing ternary complex perovskite solid solution. *J. Mater. Chem. C.* **2017**, *16*, 3916–3923. [CrossRef]
42. Shvartsman, V.V.; Lupascu, D.C. Lead-free relaxor ferroelectrics. *J. Am. Ceram. Soc.* **2012**, *95*, 1–26. [CrossRef]
43. Liu, G.; Zhang, S.; Jiang, W.; Cao, W. Losses in ferroelectric materials. *Mater. Sci. Eng. R Rep.* **2015**, *89*, 1–48. [CrossRef] [PubMed]
44. Acosta, M.; Novak, N.; Rojas, V.; Patel, S.; Vaish, R.; Koruza, J.; Rossetti, G.A.; Rödel, J. $BaTiO_3$-based piezoelectrics: Fundamentals, current status, and perspectives. *Appl. Phys. Rev.* **2017**, *4*, 041305. [CrossRef]
45. Liu, Z.; Wu, H.; Paterson, A.; Ren, W.; Ye, Z.-G. Effects of $Bi(Zn_{2/3}Nb_{1/3})O_3$ Modification on the Relaxor Behavior and Piezoelectricity of Pb $(Mg_{1/3}Nb_{2/3})$ O_3-$PbTiO_3$ Ceramics. *IEEE Trans. Ultrason. Ferroelectr. Freq. Control* **2017**, *64*, 1608–1616. [CrossRef]
46. Bokov, A.A.; Ye, Z.-G. Recent progress in relaxor ferroelectrics with perovskite structure. *J. Mater. Sci.* **2006**, *41*, 31–52. [CrossRef]
47. De La Flor, G.; Gorfman, S.; Mihailova, B. Local-scale structural response of (1-*x*)$Na_{0.5}Bi_{0.5}TiO_3$-*x*$BaTiO_3$ to external electric fields. *Appl. Phys. Lett.* **2019**, *114*, 042901. [CrossRef]